CrossMark

Role of mitochondria–cytoskeleton interactions in respiration regulation and mitochondrial organization in striated muscles

Minna Varikmaa [a,b,1], Rafaela Bagur [a,c,1], Tuuli Kaambre [d], Alexei Grichine [e], Natalja Timohhina [d], Kersti Tepp [d], Igor Shevchuk [d], Vladimir Chekulayev [d], Madis Metsis [b], François Boucher [c], Valdur Saks [a,d], Andrey V. Kuznetsov [f], Rita Guzun [a,g,*]

[a] INSERM U1055, Laboratory of Fundamental and Applied Bioenergetics, Joseph Fourier University, Grenoble, France
[b] Tallinn University of Technology, Faculty of Science, Centre for Biology of Integrated Systems, Estonia
[c] Experimental, Theoretical and Applied Cardio-Respiratory Physiology, Laboratory TIMC-IMAG, Joseph Fourier University, Grenoble, France
[d] Laboratory of Bioenergetics, National Institute of Chemical Physics and Biophysics, Tallinn, Estonia
[e] Life Science Imaging — In Vitro Platform, IAB CRI U823 Inserm, Joseph Fourier University, Grenoble, France
[f] Cardiac Surgery Laboratory, Department of Heart Surgery, Innsbruck Medical University, Innsbruck A-6020, Austria
[g] Department of Rehabilitation and Physiology, University Hospital Grenoble, France

ARTICLE INFO

ABSTRACT

The aim of this work was to study the regulation of respiration and energy fluxes in permeabilized oxidative and glycolytic skeletal muscle fibers, focusing also on the role of cytoskeletal protein tubulin βII isotype in mitochondrial metabolism and organization. By analyzing accessibility of mitochondrial ADP, using respirometry and pyruvate kinase–phosphoenolpyruvate trapping system for ADP, we show that the apparent affinity of respiration for ADP can be directly linked to the permeability of the mitochondrial outer membrane (MOM). Previous studies have shown that MOM permeability in cardiomyocytes can be regulated by VDAC interaction with cytoskeletal protein, βII tubulin. We found that in oxidative soleus skeletal muscle the high apparent K_m for ADP is associated with low MOM permeability and high expression of non-polymerized βII tubulin. Very low expression of non-polymerized form of βII tubulin in glycolytic muscles is associated with high MOM permeability for adenine nucleotides (low apparent K_m for ADP).

© 2013 Elsevier B.V. All rights reserved.

1. Introduction

Striated muscles such as cardiac and skeletal muscles have a common contractile unit named sarcomere and similar mechanism of contraction based on the conversion of free energy of ATP hydrolysis in ATPase reaction into mechanical energy for contraction. In cardiac cells, structural and functional organization of metabolism allowing connection of ATP-consuming sites such as sarcomere, sarcoplasmic reticulum and subsarcolemmal ion pumps with ATP-synthesizing systems was named intracellular energetic units (ICEUs) [1–3]. In mitochondria the energy transfer is carried out by mitochondrial interactosome (MI) supercomplex [1,4]. This complex is situated at the contact sites of the outer and inner mitochondrial membranes (MIM) and is composed of ATP synthasome (including ATP synthase, coupled to the respiratory chain complexes, adenine nucleotide translocase (ANT) and inorganic phosphate carrier), mitochondrial creatine kinase (MtCK) and voltage dependent anion channel (VDAC), interacting with cytoskeletal protein

βII tubulin and possibly with some other cytoskeletal proteins [1,4–6]. The restriction of adenine-nucleotides diffusion at the level of MOM creates a basis for the compartmentalization of energy transfer within ICEUs [7,8]. The intracellular energy flux within ICEUs is supported by phosphocreatine/creatine kinase (PCr/CK) pathway and the transfer of phosphoryl groups mainly occurs via the system of various specifically localized isoenzymes of CK and other phosphoryl-transferring kinases [2,7–9].

These mechanisms have been shown mostly for cardiac cells, but the information regarding the regulation of respiration and control of energy fluxes in various skeletal muscles is still limited. According to the myofibrillar ATPase activity, enzyme pattern and mitochondrial content, muscle fibers can be divided into three main groups: 'slow twitch oxidative fiber' (type I), 'fast twitch oxidative' (type IIA) and 'fast twitch glycolytic' fibers (types IIB, IIX) [10]. Slow twitch oxidative muscles such as m. soleus (consisting of about 84% type I and 7% type IIA fibers) display relatively low ATPase activity and large capacity for oxidative phosphorylation with high mitochondrial content (still significantly lower than in the heart) [11]. They are able to sustain low intensity workloads for long periods of time. Fast glycolytic muscles, i.e. white portion of rats m. gastrocnemius (GW) (consisting of about 92% type IIB fibers) display three- to fivefold higher ATPase activity than oxidative muscles and are

able to support high intensity workloads for short periods of time [11,12]. As a general rule, skeletal muscles consist of mixture of oxidative and glycolytic muscle fibers. For example, red portion of gastrocnemius muscle (GR) is formed of 51% type I and 35% type IIA fibers [11]. Relative to the cell volume mitochondria occupy about 35% in cardiac myocytes, about 6–10% in oxidative and only 1% in glycolytic skeletal muscle cells [13–15]. It has been shown that isolated mitochondria from oxidative and glycolytic muscles display similar characteristics. For instance, there are similar maximal rates of ADP-stimulated respiration per mg of mitochondrial protein and similar activities of isolated respiratory chain complexes [16,17]. Proteomic analysis of isolated mitochondria has revealed only few differences of protein contents between them [17]. However, several experimental studies using cell permeabilization have indicated distinct patterns of mitochondrial regulation in oxidative and glycolytic muscle fibers. Major differences were found in the apparent affinity of oxidative phosphorylation for ADP. In particular, the apparent K_m for ADP in the heart and *m. soleus* has been shown to be an order of magnitude higher than that of glycolytic muscles [12,18–20]. Several recent studies suggested that it can be associated with different permeability of MOM for ADP regulated by the binding of heterodimeric αβ tubulin to VDAC [1,21–25]. Our recent immunochemical studies of the distribution of β tubulin isoforms in cardiomyocytes linked this phenomenon to the presence of mitochondria-specific isoform of βII tubulin [26,27].

In the present work, we studied: i) the relationship between the apparent K_m for ADP and MOM permeability in skeletal muscle fibers by estimating respirometrically accessibility of mitochondrial ADP in the presence of excess of PK–PEP trapping system for external ADP, ii) flux control that different MI complexes exert on the total energy flux in oxidative and glycolytic permeabilized skeletal muscle fibers and iii) the dependence of MOM permeability on βII tubulin distribution, considering polymerization–depolymerization equilibrium of tubulin and mitochondrial arrangement. We hypothesized that the differences in mitochondrial affinity for ADP between oxidative and glycolytic muscles might be explained by different distribution pattern and/or by different free protein content of βII tubulin which may participate in feedback regulation of mitochondrial metabolism.

2. Material and methods

2.1. Laboratory animals and chemicals

Male Wistar rats weighing 150–200 g were used in the experiments. The animals were housed at constant temperature (22 °C) in environmental facilities with a 12:12 h light–dark cycle. Animal procedures were approved by "Comité d'éthique pour l'expérimentation animale" of Grenoble (33_LBFA-VS-01) and National Committee for Ethics in Animal Experimentation (Estonian Ministry of Agriculture).

2.2. Preparation of permeabilized fibers

Rats were anaesthetized with sodium pentobarbital (40–50 mg kg^{-1}) intraperitoneal injection, decapitated and, the muscles of interest were placed into a plastic Petri dish containing ice-cold isolation solution A of the following composition: 10 mM Ca-EGTA buffer (2.77 mM of CaK$_2$EGTA + 7.23 mM K$_2$EGTA) free concentration of calcium 0.1 μM, 20 mM imidazole, 20 mM taurine, 49 mM K-MES, 3 mM K$_2$HPO$_4$, 9.5 mM MgCl$_2$, 5.7 mM ATP, 15 mM PCr, pH 7.1. Muscle-fiber bundles were separated from each other using extra-sharp antimagnetic forceps under a microscope of a cold light source. To study the regulation of mitochondrial respiration of muscle, fibers were permeabilized by saponin treatment (50 μg/mL) keeping the mitochondrial membranes intact [20,28]. The permeabilization procedure was followed by triple wash in ice-cold Mitomed solution containing 0.5 mM EGTA, 3 mM MgCl$_2$, 60 mM K-lactobionate, 3 mM KH$_2$PO$_4$, 20 mM taurine, 20 mM HEPES, 110 mM sucrose, 0.5 mM dithiothreitol, 2 mg mL^{-1} fatty acid free

BSA, pH 7.1. The aim is to wash out saponin and other metabolites, especially traces of ADP or ATP, and proteases released for damaged lysosomes due to the saponin effect. To protect fibers of the proteolytic effect of lysosomal enzymes during experiments Mitomed is supplemented with 2 mg mL^{-1} BSA and leupeptin 1 μM [29]. The studied muscles are as follows: soleus; red portion of gastrocnemius muscle (GR), white portion of gastrocnemius muscle (GW), extensor digitorum longus (EDL), and left ventricle muscle (LV).

Heart mitochondria were isolated as described previously in [30] using trypsin.

2.3. Measurements of oxygen consumption

The rates of oxygen uptake were determined with a high-resolution respirometer (oxygraph-2 K, OROBOROS Instruments, Austria) in Mitomed solution supplemented with 5 mM glutamate and 2 mM malate. These measurements were carried out at 25 °C and taken the solubility of oxygen as 240 nmol mL^{-1} [31]. The respiration rates of permeabilized cardiomyocytes were expressed in nmol of oxygen consumed per minute per nmol of cytochrome aa3. The content of mitochondrial cytochrome aa3 was measured spectrophotometrically according to the method described previously [4]. Measurements of cytochrome aa3 content in skeletal muscles were limited by the necessity to increase the amount of the samples because of their lower mitochondrial content. As a result, decreased optical density compromised the quality of cytochrome aa3 measurements in spectrophotometry. The respiration rates of permeabilized muscle fibers were expressed in nmolO$_2$ min^{-1} mg^{-1} dry weight fibers. Wet fibers were dried at 100 °C for 24 h. Respiration rates were not compared between different muscles, but inside each muscle fiber-type between ADP- and Cr-stimulated respirations.

One of the most reliable quality tests of the intactness of membrane structures for permeabilized fibers is the cytochrome c test used to check the integrity of MOM [28]. Measurement of cytochrome c release from mitochondria in permeabilized cells can be studied qualitatively by Western blot and quantitatively by spectrophotometry. Western blot analysis is highly specific for cytochrome c, but it's time-consuming and requires separate labeling of isolated mitochondrial and cytosolic fractions. Isolation of mitochondria embedded into muscle fibers cytoskeleton gives two fractions: light or damaged mitochondria with increased MOM permeability and cytochrome c release and intact mitochondria. Time is also a very important factor because the aim of the cytochrome c release study is to select permeabilized fibers with intact mitochondria for the measurements of oxygen consumption. Permeabilized fibers or cells were used for respirometry studies during the first 3 h after permeabilization. Appaix et al. (2000) developing method of spectrophotometric measurement of cytochrome c in permeabilized cells showed that their results were equal to those of oxygraphic determination of cytochrome c-dependent respiration of permeabilized cardiomyocytes [32]. This experiment is carried out in KCl-solution (125 mM KCl, 20 mM HEPES, 5 mM KH2PO4, 3 mM Mg acetate, 0.4 mM EGTA, 0.3 mM DTT) supplemented with respiratory substrates (glutamate and malate) and 2 mM of ADP to get the maximal rate of respiration. Cytochrome c is a highly soluble hemoprotein of the respiratory chain that transfers electrons and is loosely associated with the outer side of the inner mitochondrial membrane. If MOM is disrupted, cytochrome c leaves mitochondria decreasing maximal respiration rate and consequently, in this situation its addition in presence of ADP will increase respiration rate. Fig. 1A shows high maximal rates of ADP-stimulated respiration and high respiration control ratio (RCR) which is estimated by the ratio between maximal ADP-stimulated and basal respiration rates (V_{maxADP}/V_0), and indicates preserved flux through the electron transport chain after saponin permeabilization. Subsequently, the addition of carboxyatractyloside (CAT) gives us information about the integrity of mitochondrial inner membrane (MIM). CAT inhibits in irreversible way ANT interrupting ATP/ADP exchange
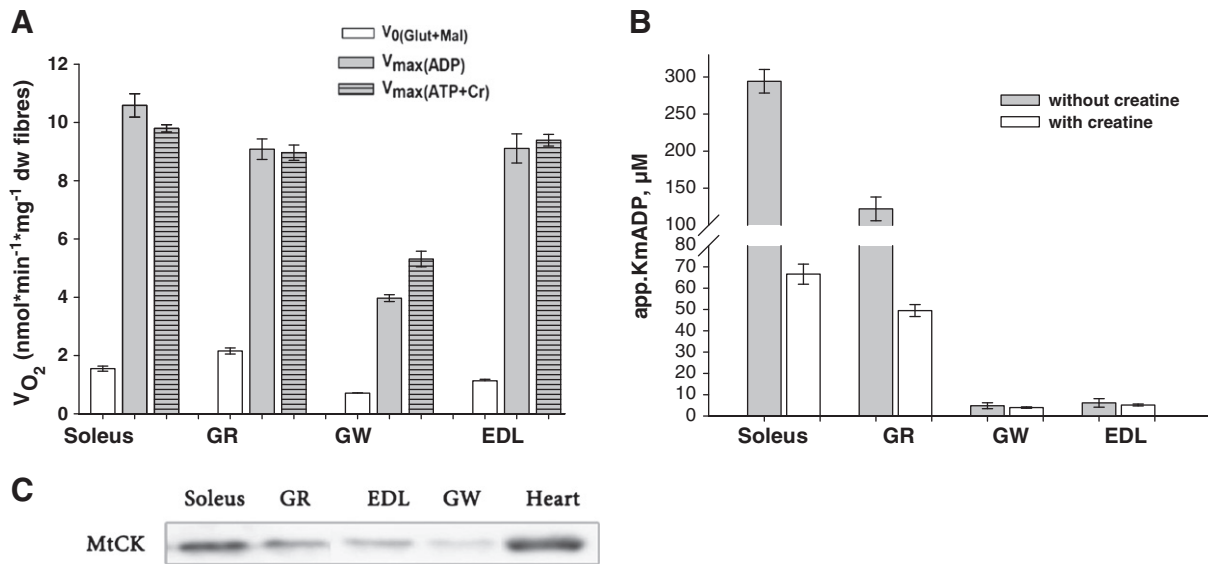
Fig. 1. Respiration rates and regulation of mitochondrial function in permeabilized skeletal muscle fibers. A) Basal (V_0) and maximal respiration rates stimulated by ADP ($V_{max}ADP$) or by creatine in the presence of ATP ($V_{max}(ATP + Cr)$). In the presence of ATP and creatine mitochondrial respiration can be stimulated by ADP generated from the hydrolysis of ATP in ATPase reactions and by ADP re-cycled in the activated MtCK reaction coupled with ANT. B) The apparent K_m for ADP of Soleus; EDL, extensor digitorum longus; GR, gastrocnemius red; GW, gastrocnemius white and LV, left ventricle is estimated in the absence and in the presence of 30 mM creatine. C) Western blot analysis of mitochondrial creatine kinase (MtCK) in heart and skeletal muscles reveals the expression of protein in all samples studied. Equal loading (25 μg) of protein was confirmed by membrane Ponceau staining. The data are representative of at least three independent experiments.

between mitochondrial matrix and intermembrane space. Therefore, if MIM is intact, addition of CAT decreases oxygen consumption rate back to initial level. In our experiments only fibers with intact mitochondria and with a high maximal rate of respiration were used for experiments. All experiments were performed in the presence of protease inhibitor in order to avoid the influence of lysosomal proteolysis on kinetic parameters described by Perrey et al. [29,33].

2.4. Determination of flux control coefficients

Metabolic control analysis (MCA) allows quantitative determination of the degree of control that a given enzyme exerts on metabolic flux [34,35]. To understand mechanisms by which a given enzyme exerts high or low control on metabolic pathway, its flux control coefficient (FCC) is evaluated. The flux control coefficient is the degree of control that the rate (v) of a given enzyme i exerts on flux J. Groen in 1982 derived a method to determine experimentally the FCC using titration curves with specific enzyme inhibitors. As the amount of inhibitor tends to zero the response of the flux to the inhibitor can be expressed in MCA terms [34]. The flux control coefficient of enzyme i on flux J is given by the symbol $C_{V_i}^J$ and defined according to the equation [35]:

$$C_{V_i}^J = \left(\frac{dJ}{dv_i}\right) / \left(\frac{J}{v_i}\right) = \frac{d \ln J}{d \ln v_i}$$

in which (dJ/dv_i) describes the variation in flux (J) when an infinitesimal change takes place in the enzyme i concentration or activity. In practice, the infinitesimal changes in v_i are undetectable, and hence measurable noninfinitesimal changes are undertaken. If a small change in v_i promotes a significant variation in J, then this enzyme exerts a high flux control. In contrast, if a rather small or negligible change in the flux is observed when v_i is greatly varied then the enzyme does not exert a significant flux control. For the case of irreversible specific inhibitor, an estimation of FCC value is given by Groen et al. (1982) and Moreno-Sanches et al. (2008) as [34,36]:

$$C_{V_i}^J = \left(\frac{\Delta J}{\Delta I}\right) * \left(\frac{I_{max}}{J_0}\right)$$

where ($\Delta J / \Delta I$) is initial slope of the stepwise inhibition of oxygen respiration graph, I_{max} is the inhibitor concentration giving complete inhibition, and J_0 is the initial steady-state flux value. The flux control coefficients in permeabilized skeletal fibers were determined by using graphical method described by Fell [35].

The inhibitors used in our work and considered as pseudo-irreversible and non-competitive in these conditions were: carboxyatractyloside (CAT) for ATP/ADP transporter, oligomycin for ATP synthase, rotenone for complex I, antimycin-A (ANM) for complex III, sodium cyanide (NaCN) for complex IV and 1-Fluoro-2,4-dinitrobenzene (DNFB) for MtCK. The respiration rates were measured in the presence of glutamate, malate and succinate. High quality fiber preparations with respiratory control ratio (RCR = V_{maxADP} / V_0) and acceptor control ratio (ACR = $V_{max(ATP + Cr)} / V_0$) higher than five were used (Table 2).

2.5. Western blot analysis

Free and polymerized tubulins were assessed using Microtubule/ Tubulin In Vivo Assay Kit (Cytoskeleton). Tissue powder was suspended in 37 °C microtubule stabilization buffer (5 mM MgCl₂, 1 mM EGTA, 0.1 mM ATP, 100 mM PIPES, 30% glycerol, 0.1% Nonidet-P40, 0.1% Triton X-100, 0.1% Tween-20, 0.1% β-mercaptoethanol, 0.001% antifoam, 0.1% BME, pH 7.4, Complete Protease Inhibitor Cocktail (Roche)), homogenized using 25G syringe and centrifuged at 37 °C for 5 min at 2000 ×g. Supernatants were centrifuged at 100,000 ×g for 30 min at 37 °C to yield supernatant containing free tubulin and pellet containing polymerized tubulin. The pellet was resuspended in Brinkley buffer (80 mM PIPES, 1 mM MgCl₂, 1 mM EGTA) containing 4 M urea, incubated on ice for 45 min and centrifuged at 12,000 ×g for 10 min to remove any insoluble material. The protein concentration was determined using the Pierce BCA Protein Kit. For assessment of MtCK expression, only soluble protein extract was used. Protein samples were resuspended in 1× SDS sample buffer containing 10% β-ME, heated at 95 °C for 5 min and 50 μg of protein was loaded onto 12% polyacrylamide gels. Electrophoresis was performed on the Mini Protean II from BioRad in the Tris–tricine buffer solution. Blotting of the unstained gels was performed on the Trans-Blot SD Semi-Dry Transfer Cell (BioRad) using PVDF membranes (Millipore). The blotting buffer contained 48 mM Tris, 39 mM glycine, 0.1% SDS and 20% methanol.

Table 1
Respiratory parameters of permeabilized skeletal muscle fibers.

	V_0	V_{max} (ADP)	V_{max} (ATP + Cr)	K_mADP	K_mADP (+Cr)	PK–PEP inhibition
	$nmolO_2\ min^{-1}\ mg^{-1}$ dry weight fibers			μM		%
Soleus	1.55 ± 0.09	10.6 ± 0.4	9.8 ± 0.1	294.2 ± 15.9	66.6 ± 4.7	2.2 ± 0.5
Gastrocnemius red	2.10 ± 0.08	9.1 ± 0.4	9.0 ± 0.3	122.0 ± 16.0	49.5 ± 2.8	52.8 ± 5.2
Gastrocnemius white	0.70 ± 0.01	3.8 ± 0.1	5.3 ± 0.27	4.5 ± 1.8	3.6 ± 0.3	48.6 ± 0.2
Extensor digitorum longus	1.10 ± 0.05	9.1 ± 0.5	9.4 ± 0.2	7.4 ± 1.7	5.2 ± 0.6	49.0 ± 3.0

Respiration of permeabilized skeletal muscle fibers was measured in the presence of 5 mM glutamate and 2 mM malate in Mitomed solution at 25 °C. Values are means ± SEM.

Equal protein transfer was verified by staining membrane with Ponceau solution (0.1% Ponceau S in 5% acetic acid). The membranes were blocked for 1 h in 3% BSA PBS or 0.5% skimmed milk, 0.05% Tween-20 PBS solution and treated with 1:250 rabbit polyclonal anti-MtCK (Abcam), 1:250 mouse monoclonal anti-βII tubulin (Abcam) and 1:500 rabbit polyclonal anti-β-tubulin (Abcam) antibodies 2 h at room temperature. Immunoblots were detected by 1:45,000 anti-mouse or 1:1000 antirabbit secondary antibodies conjugated to peroxidase (IgG HRP; Abcam). Detection was conducted using chemiluminescence kit (SuperSignal West Dura Extended Duration substrate).

2.6. Immunolabeling of muscle fibers

Labeling of cytoskeletal and mitochondrial proteins was performed on intact rat skeletal or heart left ventricular muscle fibers in suspension. Fibers were fixed in 4% paraformaldehyde in PBS at 37 °C for 15 min. For immunolabeling of mitochondrial proteins (VDAC, MtCK) heat-mediated antigen retrieval was performed by incubating fibers in Antigen Retrieval Buffer (10 mM Tris, 5% urea, pH 9.5) at 95 °C for 3 min. After washing with PBS fibers were permeabilized with 1% Triton X-100 at room temperature for 30 min., washed again with PBS, and blocked in PBS solution containing 2% BSA (bovine serum albumin) for
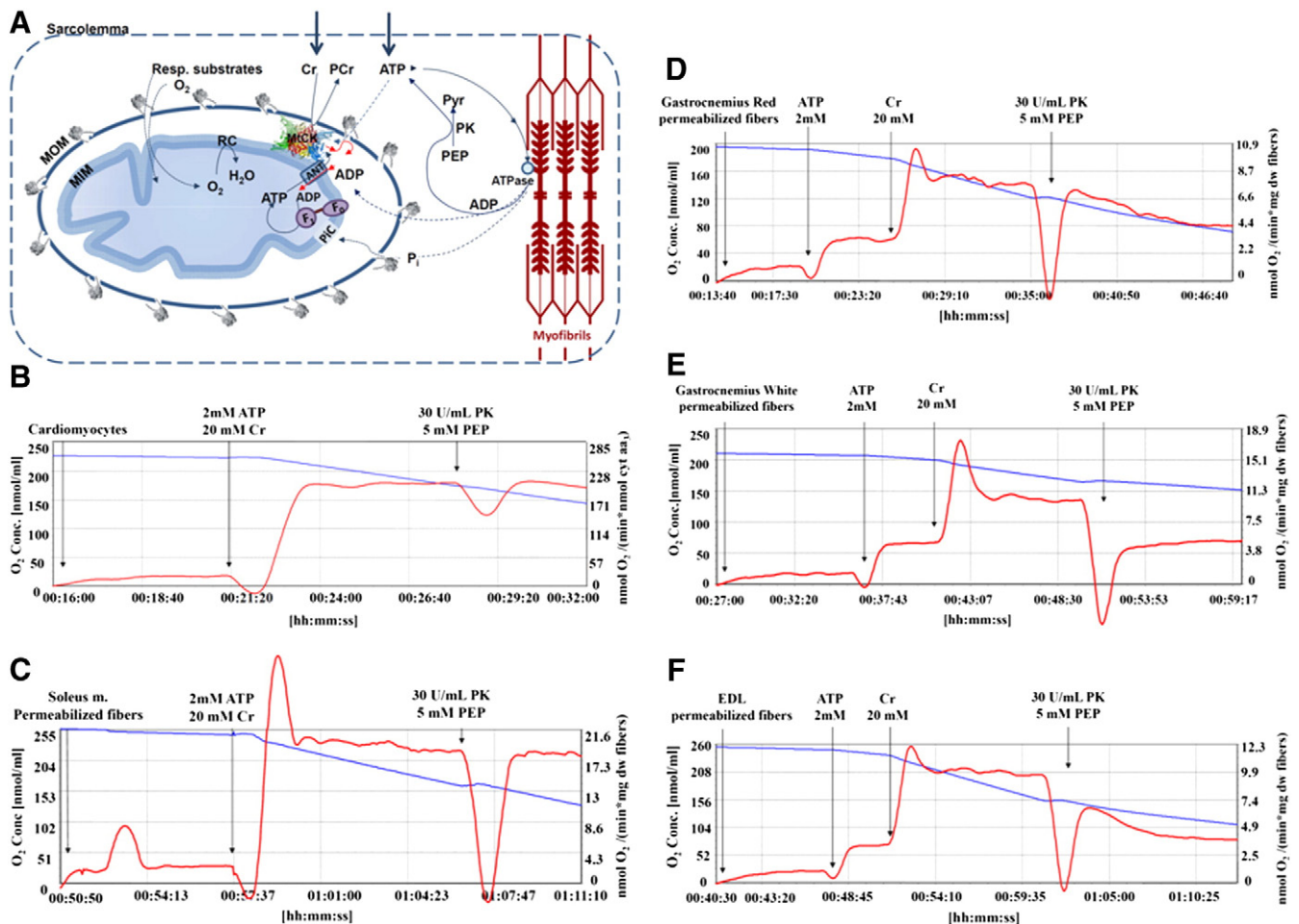
Fig. 2. Measurement of ADP fluxes from mitochondria in situ, in permeabilized muscle cells. A) Scheme showing mitochondrion in permeabilized cell. MOM — mitochondrial outer membrane. Exogenous ATP is hydrolyzed by cellular ATPases into extra-mitochondrial ADP and inorganic phosphate (Pi). Mitochondrial (MtCK) in the presence of creatine and ATP locally produces endogenous intra-mitochondrial ADP. The system is supplemented with phosphoenolpyruvate (PEP) and pyruvate kinase (PK) which remove extramitochondrial ADP produced by intracellular ATP consuming reactions and continuously regenerate extramitochondrial ATP. Endogenous intramitochondrial ADP is re-imported into the matrix for re-phosphorylation via adenine nucleotide translocase (ANT) due to its functional coupling with MtCK. B) Respiration trace of permeabilized cardiomyocytes recorded using high resolution respirometer. C–F). Measurements of ADP fluxes from mitochondria in situ in permeabilized soleus (C), gastrocnemius red, GR (D), gastrocnemius white, GW (E) and extensor digitorum longus, EDL (F) muscle fibers. The left scale and the blue trace indicate the oxygen concentration ($nmolO_2\ mL^{-1}$). The right scale and the red trace show the rate of oxygen uptake expressed in $nmolO_2\ min^{-1}\ nmol^{-1}$ cytochrome aa_3 for cardiomyocytes (B) and in $nmolO_2\ min^{-1}\ mg^{-1}$ dry weight fibers for skeletal muscle fibers (C–F). Trapping PK–PEP system did not change the respiration rates of cardiomyocytes (B) and soleus muscle fibers (C) indicating that intramitochondrial ADP is not available for PK–PEP system. In contrast, this system effectively inhibits the respiration rates of GR, GW and EDL permeabilized muscle fibers (D–F).
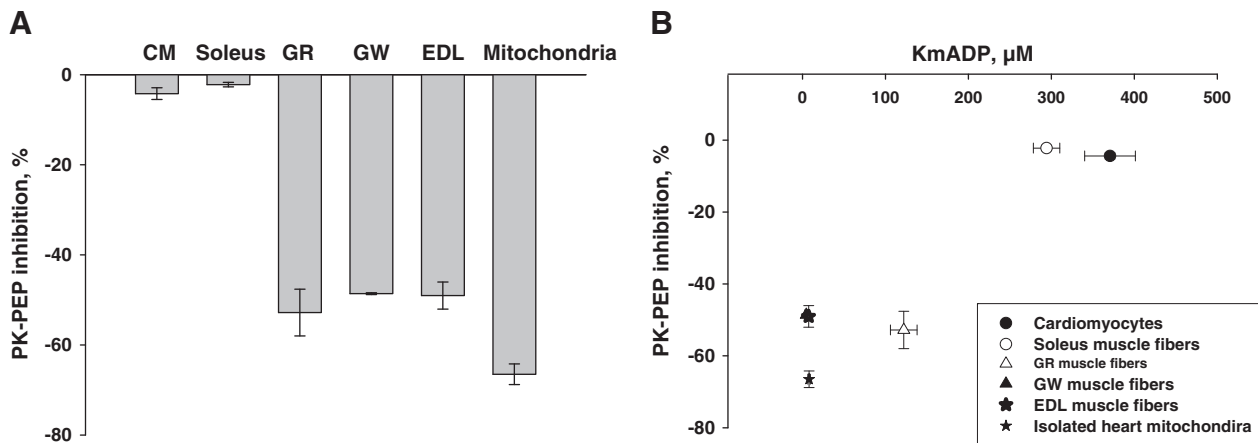
Fig. 3. Distribution of energy fluxes through the mitochondrial outer membrane studied using PK–PEP trapping system for ADP. A) The inhibition of creatine-activated respiration by the PK–PEP observed in different skeletal muscles. B) Diagram representing relationship between the inhibition of creatine-activated respiration and the apparent K_m for ADP. Low apparent affinity of oxidative phosphorylation for ADP (i.e. high app. K_mADP) is directly linked to low MOM permeability for ADP (i.e. low PK–PEP inhibition of the creatine-stimulated respiration) and vice versa.

60 min at 25 °C. Subsequently fibers were incubated overnight with primary cytoskeletal and mitochondrial antibodies. Monoclonal mouse anti-tubulin βII(β2) antibody (Abcam, ab28036) at 1:250, mouse anti-α-actinin antibody (Abcam) at 1:250, and polyclonal rabbit VDAC antibody serum (kindly provided Dr. Catherine Brenner, Universite Paris-Sud, Paris, France) at 1:1000 were used. Next day samples were rinsed 3 times for 3 min in 2% BSA solution, and stained for 2 h at room temperature with secondary antibody DyLight 488 goat anti-rabbit IgG (Abcam, ab96899) at 1:250 and Dylight 549 goat anti-mouse IgG (Abcam, ab96880) at 1:250. After washing three times with 2% BSA PBS solution and once with bidistilled water, fibers were mounted in ProLong® Gold Antifade Reagent with DAPI (Life Technologies), deposited on glass coverslips and observed by confocal microscope.

2.7. Confocal microscopy and 3D modeling

The fluorescence images were acquired by Zeiss LSM 510 confocal microscope (Carl Zeiss) equipped with a Plan-Apofluar 63×/1.30 glycerol objective. Laser excitation 488 nm was used for DyLight 488 with emission detected through a 505- to 530 band-pass filter, DyLight549 was excited at 561 nm and detected through 575- to 615 nm band-pass filter. Pinhole was adjusted to the optical slice thickness 0.27 μm for both channels. Processing of all confocal data sets was done with LSM Image Browser software performing rotation, cropping, linear contrast adjustment, channel balancing and addition of scale bar. Images presented were copy-pasted from LSM Image Browser to Photoshop CS4 without further modifications. Confocal images were collected at least 0.5 μm below the sarcolemma. Reconstruction of a 3D-model was done with Imaris software (Bitplane) using 6–7 image stacks acquired with z-step 0.27 μm.

3. Results

3.1. Inter relationship between the apparent affinity of mitochondrial respiration for ADP and MOM permeability

The apparent affinity of mitochondrial respiration for ADP was estimated by measuring ADP concentration reaching half-maximal rate of respiration (i.e. apparent affinity Michaelis constant, K_m). The apparent K_m for ADP in oxidative soleus muscle fibers was high (~300 μM, Table 1, Fig. 1B) and comparable with that of cardiomyocytes. Conversely, the apparent K_m for ADP in glycolytic GW and EDL muscle fibers was very low (~4–7 μM, Table 1, Fig. 1B) and comparable with that of isolated mitochondria. Red portion of *m. gastrocnemius* was characterized by intermediate K_mADP (about 150 μM) due to its mixed composition of slow- and fast-twitch muscle fibers. It was assumed that different apparent affinity of respiration to ADP could be explained by the restriction of ADP diffusion at the level of MOM.

The permeability of MOM was studied respirometrically measuring changes of respiration rate induced by the leakage of ADP from mitochondria. Fig. 1A summarizes main experimental conditions necessary for studying the relationship between the affinity of mitochondria respiration for ADP and MOM permeability. One of the main conditions is the equal maximal rate of creatine- ($V_{max(ATP + Cr)}$) and ADP-stimulated respiration (V_{maxADP}) measured in the presence of a saturating concentration of ADP. This similarity means that all ADP produced in MtCK reaction is returned back to matrix to stimulate respiration. As shown in Fig. 1A and Table 1 the maximal rates of ADP- and creatine-stimulated respiration are similar for each studied fiber-type. Fig. 2A shows the experimental protocol for studying ADP-fluxes through MOM in permeabilized cells. The addition of exogenous ATP stimulates mitochondrial respiration due to the production of endogenous ADP in ATPase reactions. Respiration rate stabilizes because of the establishment of the steady state between ADP production (in myofibrillar and sarcolemmal ATPase reactions) and oxidative phosphorylation. The subsequent addition of creatine in the presence of exogenous ATP enhances respiration rates due to the additional source of endogenous ADP generated by the MtCK reaction in intermembrane space. In this case, the respiration rate is activated and stabilized due to the recycling of ADP in mitochondria between MtCK, ANT and the mitochondrial matrix. In all cases stabilized respiration rate means steady state. In the absence of PK–PEP system, ADP issued from ATP hydrolysis in ATPase reactions and from MtCK reaction is available for mitochondrial matrix. The PK–PEP system can decrease respiration rate by phosphorylating ADP into ATP. In experiments with permeabilized cardiomyocytes and oxidative soleus muscle fibers creatine (Cr) was added concomitantly with ATP (Fig. 2B, C). In experiments with permeabilized glycolytic GR, GW and EDL muscle

Fig. 4. Metabolic flux control analysis of permeabilized soleus muscle fibers. Rates of oxygen consumption of permeabilized soleus muscle fibers recorded under conditions of: A) respiration stimulated by the addition of ADP and B) and by the addition of 20 mM of creatine in the presence of 2 mM ATP. The values of maximal respiration rates and initial fluxes (J_0) are comparable under both conditions. The PK–PEP system was added to remove the effect of exogenous ADP on the respiration. Respiration of permeabilized soleus fibers was progressively inhibited by stepwise addition of oligomycin. C) Inhibition titration curves for oligomycin, D) rotenone, E) carboxyatractyloside (CAT) and F) 1-Fluoro-2,4-dinitrobenzene (DNFB) are shown under conditions of respiration stimulated by both ADP and creatine.
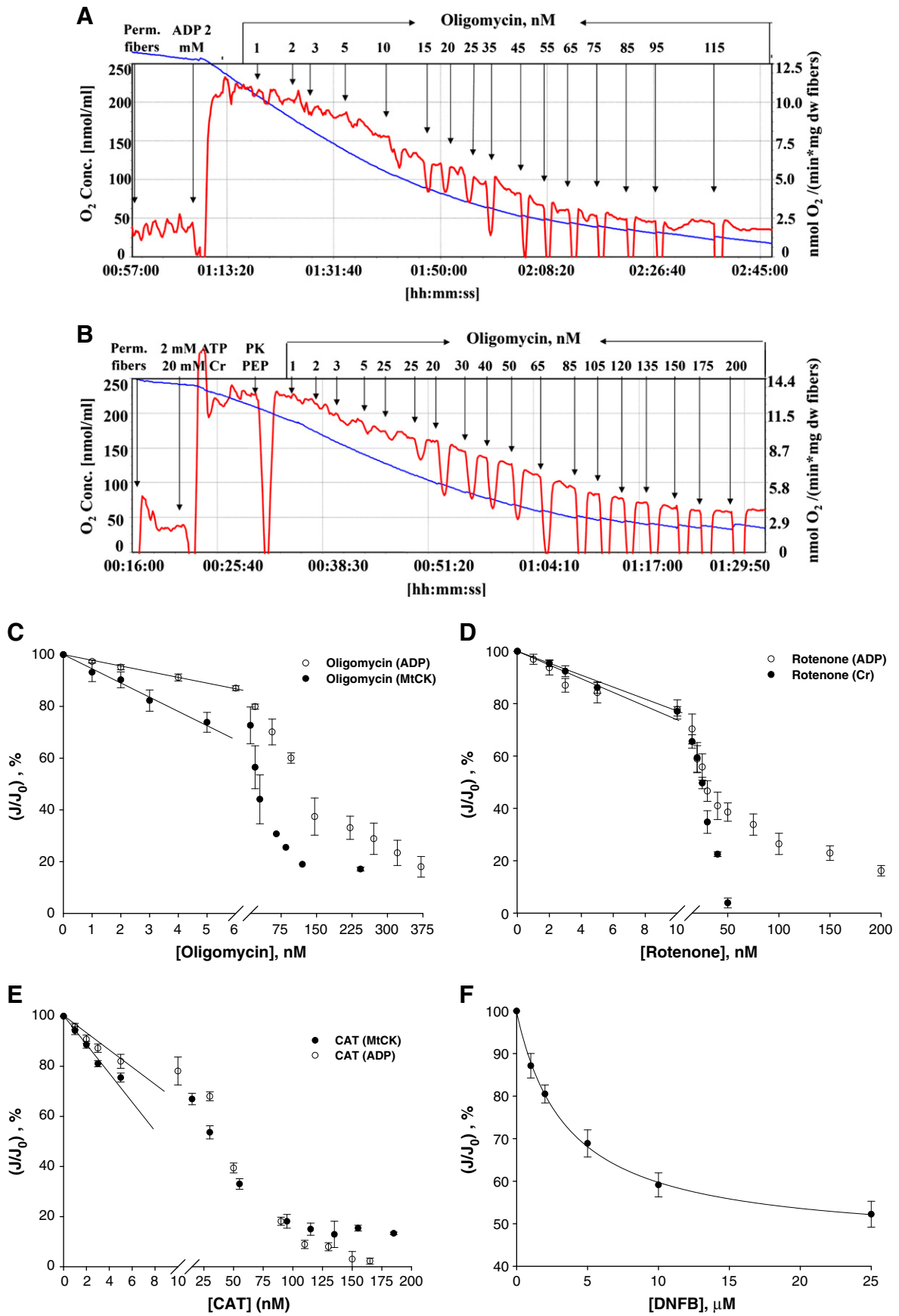
Table 2
Metabolic control analysis of permeabilized skeletal muscle fiber respiration.

	Inhibitor	Sample	ADP-stimulated respiration				Creatine-stimulated respiration			
			FCC	I_{max}, μM	J_0,nmolO$_2$ min^{-1} mg^{-1} dw fibers	RCR	FCC	I_{max}, μM	J_0,nmolO$_2$ min^{-1} mg^{-1} dw fibers	RCR
ATP/ADP carrier	Carboxy-atractyloside	Soleus m.	0.61 ± 0.04	0.11 ± 0.01	14.1 ± 1.9	6.6 ± 0.8	0.86 ± 0.05	0.12 ± 0.09	14.76 ± 2.80	6.3 ± 0.9
		GW m.	0.90 ± 0.05	0.030 ± 0.002	7.56 ± 0.30	3.90 ± 0.05				
		Cardiomyocytes*	0.20 ± 0.05	0.6			0.92 ± 0.05	0.6		
ATP synthase	Oligomycin	Soleus	0.44 ± 0.03	0.11 ± 0.01	16.17 ± 0.90	7.7 ± 1.1	0.61 ± 0.07	0.12 ± 0.07	18.42 ± 4.10	8.7 ± 2.5
		GW m.	0.67 ± 0.02	0.024 ± 0.001	9.53 ± 0.90	5.64 ± 0.61				
		Cardiomyocytes*	0.065 ± 0.01				0.38 ± 0.05			
NADH-CoQ oxidoreductase, Complex I	Rotenone	Soleus m.	0.69 ± 0.05	0.036 ± 0.001	14.6 ± 1.1	5.3 ± 0.1	0.71 ± 0.02	0.026 ± 0.001	16.8 ± 0.6	7.2 ± 0.4
		GW m.	0.54 ± 0.06	0.028 ± 0.001	12.83 ± 1.83	8.67 ± 1.61				
		Cardiomyocytes*	0.20 ± 0.04	0.1			0.64 ± 0.03	0.1		
CoQ cytochrome-c oxidoreductase, Complex III	Antimycin A	Soleus m.	0.47 ± 0.01	0.025 ± 0.002	15.4 ± 0.2	6.5 ± 0.05	0.61 ± 0.01	0.033 ± 0.003	15.4 ± 0.3	7.3 ± 0.4
		GW m.	0.82 ± 0.01	0.0200 ± 0.0004	10.92 ± 0.23	6.81 ± 0.23				
		Cardiomyocytes*	0.41 ± 0.08				0.40 ± 0.01	0.2		
Cytochrome c oxidase, Complex IV	NaCN	Soleus m.	0.73 ± 0.03	20.0 ± 2.5	15.6 ± 1.2	6.6 ± 0.7	0.94 ± 0.01	13.74 ± 2.9	14.6 ± 0.6	5.7 ± 0.6
		GW m.	0.84 ± 0.01	8.05 ± 0.45	10.44 ± 0.22	6.34 ± 0.13				
		Cardiomyocytes*	0.39 ± 0.09	75			0.49 ± 0.08	75		
Mitochondrial creatine kinase	DNFB	Soleus m.					0.76 ± 0.01	0.09 ± 0.01		
		Cardiomyocytes*					0.95 ± 0.02	40		
Sum		Soleus m.	3.05 ± 0.06				4.49 ± 0.03			
		GW m.	3.77 ± 0.02							
		Cardiomyocytes*	1.33 ± 0.31				3.84 ± 0.29			

Respiration of permeabilized skeletal muscle fibers was measured in the presence of 5 mM glutamate and 2 mM malate and 10 mM succinate in Mitomed solution at 25 °C. The ADP-stimulated respiration means that the respiration is stimulated by exogenous ADP (2 mM). The creatine stimulated respiration means that the respiration is stimulated by endogenous ADP produced in MtCK reaction within mitochondrial intermembrane space. MtCK reaction is activated by the addition of 20 mM creatine in the presence of 2 mM ATP. Extramitochondrial ADP is trapped up by system consisting of 20 IU/mL pyruvate kinase (PK) and 5 mM phosphoenolpyruvate (PEP). * — data for cardiomyocytes was taken from Tepp et al. (2011) for comparison [47]. I_{max} — inhibitor concentration giving complete inhibition, J_0 — initial flux or maximal respiration rate in the absence of inhibitor, GW.m — gastrocnemius white muscle. The estimation of the flux control coefficient (FCC) was done with n ≥ 3. Values are means ± SEM.

fibers creatine was added after the stabilization of respiration rates in the presence of exogenous ATP (Fig. 2D–F). Separate addition of creatine allowed us to highlight its role in the control of respiration in GR, GW and EDL muscles characterized by low MtCK expression (Western blot analysis from Fig. 1C). The addition of PK–PEP to permeabilized cardiomyocytes and soleus muscle fibers did not inhibit significantly the maximal rate of creatine-stimulated respiration (Fig. 2B and C). In contrast, in permeabilized GR, GW and EDL muscle fibers, the addition of PK–PEP system decreased creatine-stimulated respiration by about 50% (Fig. 2D–F).

Fig. 3 shows the relationship between PK–PEP inhibition of creatine-stimulated respiration, which is used to bring to evidence the MOM permeability and the apparent K_m for ADP in different permeabilized muscle fibers and cardiomyocytes in comparison with isolated heart mitochondria. To compare the inhibition effect of PK–PEP in muscle fibers with different amount of mitochondria and proteins, we expressed it as a percentage of the maximal Cr-stimulated respiration rate (Fig. 3A). Very low inhibition of Cr-stimulated respiration by PK–PEP system in permeabilized cardiomyocytes and oxidative soleus muscle fibers (about 2–5%, Fig. 3A) is related to high apparent K_m for ADP (Fig. 3B). In contrast, the low app. K_m for ADP in GW and EDL muscles is associated with high ADP-trapping effect of PK–PEP system (Fig. 3A and B). The red portion of gastrocnemius muscle, due to its mixed composition of fiber-types, has an intermediate apparent K_mADP between that of oxidative and glycolytic fiber-types and a high PK–PEP inhibition.

3.2. Study of energy fluxes in permeabilized skeletal muscle fibers using metabolic control analysis

The quantitative study of the control that the respiratory chain complexes (I, III, IV), ANT and ATP synthase exert on the energy flux in oxidative soleus and glycolytic GW permeabilized muscle fibers was performed using metabolic control analysis under conditions of ADP-stimulated respiration. Additionally, the role of MtCK in the control of energy flux in soleus permeabilized muscle fibers was studied using experimental setting described in Fig. 2A (i.e. Cr-stimulated respiration). We could not apply the same protocol to GW muscle fibers because of the inhibitory effect of PK–PEP on creatine-stimulated respiration. After the addition of PK–PEP system, the resulting lower level of creatine — in comparison with ADP — stimulated respiration did not allow us to compare the flux control coefficients of the same complexes measured under both conditions.

Fig. 4A and B shows two respirometry traces and Fig. 4C summarizes statistics of the oligomycin stepwise inhibition of ADP- (Fig. 4A) and Cr-stimulated respiration (Fig. 4B) in permeabilized soleus muscle fibers. The inhibition of the initial (J_0) flux in the presence of activated MtCK, which was faster and induced with lower amounts of oligomycin, indicates to the higher control that ATP synthase exerts on the flux when respiration is controlled by Cr in comparison with direct control by ADP (Fig. 4A–C, Table 2). Similarly higher FCC in the presence of activated MtCK in comparison with ADP-stimulated respiration was found for ANT (Fig. 4E, Table 2). High flux control coefficients of respiratory complexes (I, III, IV) indicate their relevance in the control of the metabolic flux (Fig. 4, Table 2). Table 2 additionally shows flux control coefficients of all studied complexes for permeabilized soleus and GW muscle fibers. Concentrations of rotenone, antimycin and oligomycin necessary to achieve the maximal rates of inhibition of ADP-stimulated respiration were in good agreement with previously published data (Table 2) [12,37–40]. Flux control coefficients of ATP synthase and ANT estimated for soleus muscle fibers were also consistent with previously reported results. Conversely, flux control coefficient of complex IV (NaCN titration) estimated for *m. soleus* fibers was higher than that reported in literature [41]. This difference can be explained by higher initial flux (J_0) due to the utilization of respiratory substrates for complexes I and II. The strong dependence of control coefficients on the flux was previously described by Kunz et al. [39]. The sum of flux control coefficients in both muscle-types and

under ADP- and Cr-stimulated respiration largely exceeding unity suggests organization of the respiratory chain complexes I, II, IV, ATP synthase and ANT into supercomplex (Table 2).

3.3. The expression and distribution of βII tubulin in striated muscle fibers

According to several recent reports the MOM permeability for adenine nucleotides is governed by the interaction of VDAC with heterodimeric tubulin [21–27]. The expression of free and polymerized βII tubulin was assessed by Western blot analysis. The content of free βII tubulin was highest in oxidative heart and soleus muscles, whereas in mixed-type GR and glycolytic EDL and GW muscles its levels are markedly lower (Fig. 5A). To assess the content of polymerized βII tubulin, extraction of cold-insoluble tubulin in up to 2 mM $CaCl_2$ or 4 M urea containing resuspension buffer was tested. In both cases, no polymerized βII tubulin was detected in skeletal muscles and only minor levels were observed in heart muscle (Fig. 5A). Similar observation was reported earlier for nerve axons, where large amounts of tubulin were left unextracted with high concentration of urea, Ca^{2+}, colchicine, and nocodazole [41]. Of note, βII tubulin isoform accounts for over 50% of total β-tubulin present in nerve axons [42]. Since quantitative estimation of polymerized to free βII tubulin ratio of was not possible due to its scarcity in glycolytic muscles, we analyzed additionally the content of total β tubulin. Both forms of free and polymerized β tubulin were higher in heart and oxidative soleus muscles than in GR, EDL and GW (Fig. 5A). The densitometric analysis showed that polymer to dimer ratio of total β tubulin is almost equal across muscle fiber types with estimated values as follows: heart 0.06 ± 0.015; soleus 0.074 ± 0.03; GR 0.043 ± 0.007; EDL 0.066 ± 0.01 and GW 0.034 ± 0.005 (Fig. 5B).

Intracellular localization of βII tubulin relative to mitochondria was studied using co-immunolabeling of fixed muscle fibers with antibodies for βII tubulin and for mitochondrial protein VDAC, and assessed their localization by confocal microscopy. The presence of βII tubulin was detected in all studied muscle fiber types, including EDL and GW. In heart and soleus muscle fibers βII tubulin appeared as thick segregated bundles aligned closely to mitochondria between Z-lines as shown in Fig. 6A–C, D–F and further highlighted in higher magnification image of heart fibers in Fig. G–I. In gastrocnemius and EDL muscle fibers (image shown only for GW muscle fibers) βII tubulin is seen as thin continuous filaments situated at Z-lines and similarly to heart and soleus covered by mitochondria (Fig. 8A–C, E–G, D, H, I).

Co-immunolabeling of β-tubulin and α-actinin showed that in oxidative muscles β-tubulin is concentrated entirely at the area between Z-lines, similarly to βII isoform, while in GW and EDL (image shown only for GW) two subpopulations of β-tubulins are present (Fig. 9). One at the level of Z-lines, similarly to βII tubulin, and second at the level of A-band, as in oxidative muscles.

All together these results lead us to believe that differences in MOM permeability for ADP stem from the variances in expression levels of βII tubulin relative to mitochondria.

4. Discussion

The apparent K_m for ADP in permeabilized cardiomyocytes and oxidative soleus muscle fibers is an order of magnitude higher than in glycolytic GW and EDL muscles (Table 1, Fig. 1B) [12,43]. We hypothesized that the differences in mitochondrial affinity for ADP between oxidative and glycolytic muscles might be explained by different distribution pattern and/or by different free protein content of βII tubulin.
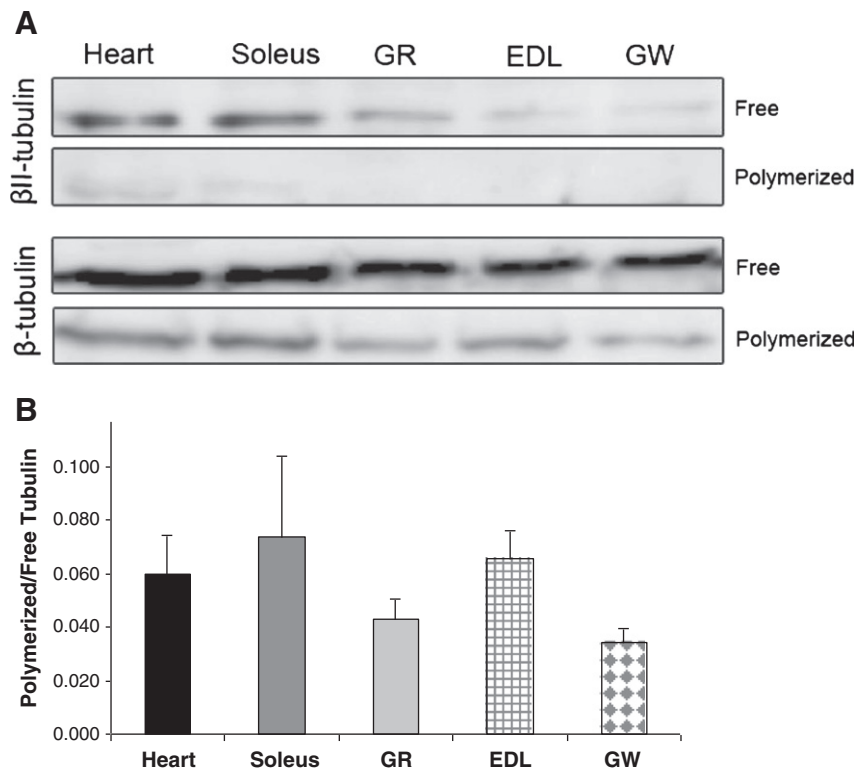
Fig. 5. Western blot analysis of free and polymerized βII tubulin and total β tubulin in rat heart and skeletal muscles. (A) Upper panel shows immunoblot of free and polymerized βII tubulin and total β tubulin in soluble and insoluble muscle extracts prepared under microtubule stabilizing conditions. (B) Lower panel shows densitometric quantification of the total β-tubulin in the soluble and insoluble fractions. Equal proportion of free and polymerized samples were loaded onto the lanes and an equal amount (35 μg) of protein for each muscle sample. The data shown are representative of 3–4 independent experiments. Statistical comparison was done by one-way ANOVA and results represent means ± SEM. P < 0.05.
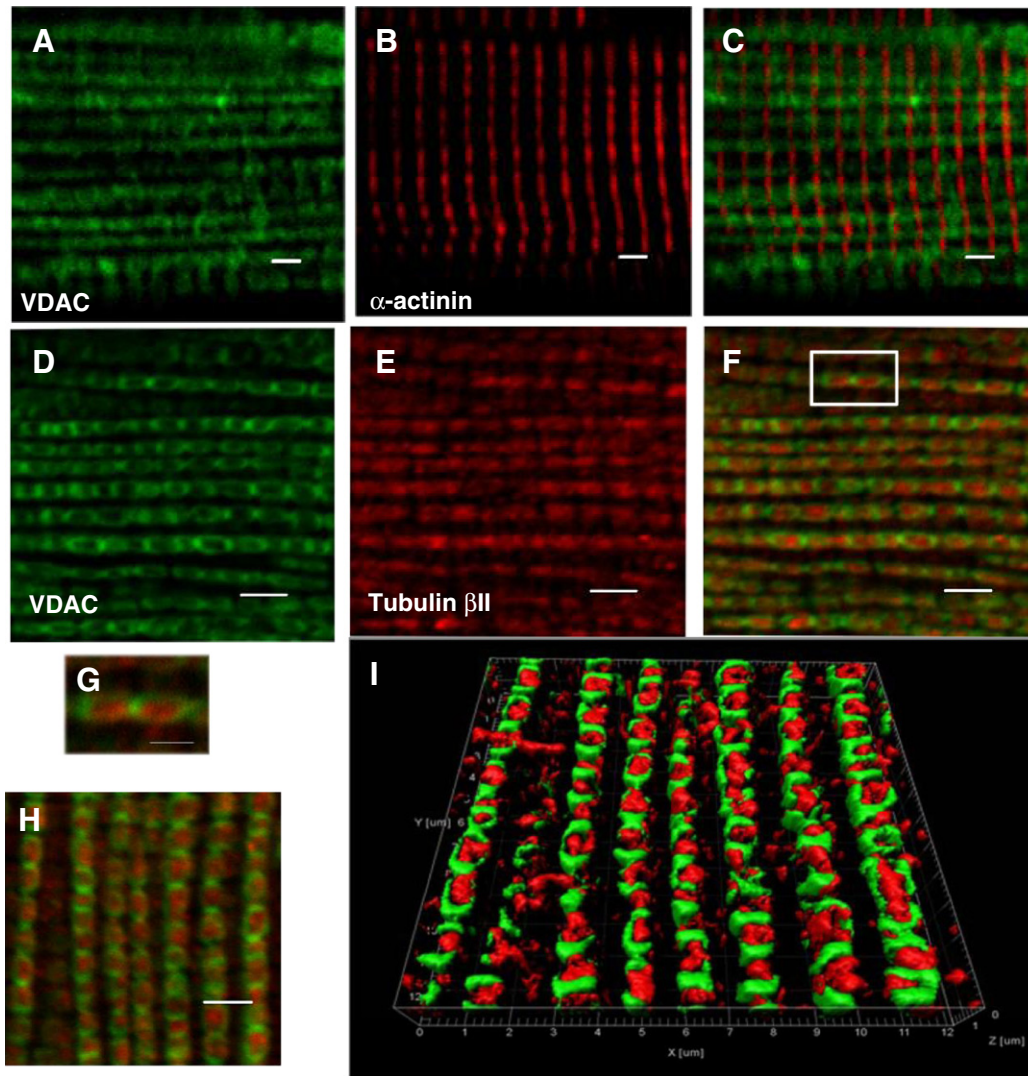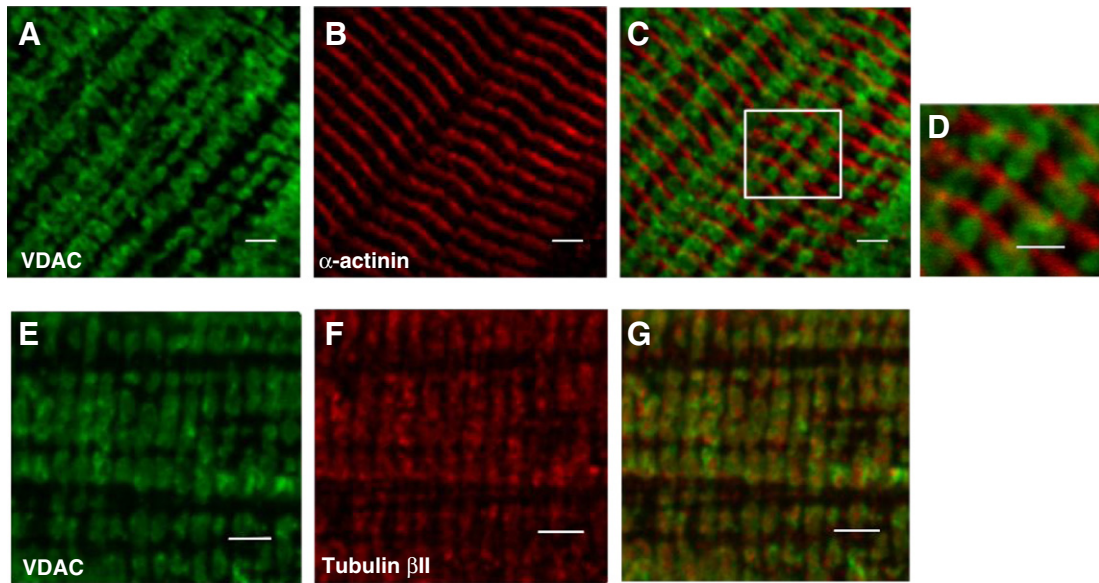
Fig. 6. Confocal microscopy images of mitochondria and βII tubulin arrangement in adult cardiac muscle fibers. Optical slices of fibers co-immunolabeled for VDAC (A) and α-actinin (B), and for VDAC (D) and βII tubulin (E) are obtained at least 0.5 μm beneath sarcolemma and specimens are all oriented so that the long axis of the fiber is directed longitudinally. Images show that both mitochondria and βII tubulin are arranged regularly between Z-lines. Scale bar 2 μm. I) Three-dimensional reconstruction of confocal image represented in Fig. 5H). Heart fibers immunolabeled for VDAC and βII tubulin were scanned at 0.27-μm intervals along the z-axis (maximum 10 planes, depending on the signal intensity) and 3D surface model was reconstructed by Imaris software (Bitplane). Scale bar, 2 μm. Image is oriented so that the long axis of the fiber is directed along y-axes.

4.1. Inter relationship between the apparent affinity of mitochondrial respiration for ADP and MOM permeability

The dependence of the apparent affinity of respiration for ADP on the MOM permeability was previously hypothesized based on kinetic analysis of respiration control by ADP [12]. We studied ADP fluxes through MOM in permeabilized fibers using PK–PEP system which competes with oxidative phosphorylation for ADP produced in mitochondrial intermembrane space by activated MtCK reaction [44]. In glycolytic gastrocnemius and EDL muscles, characterized by low apparent K_mADP the addition of PK–PEP system decreased Cr-stimulated respiration by about 50% of $V_{max(ATP + Cr)}$ (Fig. 3B). Effect observed in glycolytic muscles can be due to neither saponin permeabilization nor low MtCK expression. MOM intactness was confirmed by the absence of stimulatory effect of exogenous cytochrome c on the maximal ADP-stimulated respiration rate. Using electron microscopy it was shown that 100 μg/mL of saponin used to permeabilize cells for 30 min did not alter MOM connections with cytoskeleton [45]. However, taking into account that by removing cholesterol from lysosomal membranes,

saponin hypothetically could increase cytoskeleton proteolysis, all experiments were lead in the presence of protease inhibitors [29,33]. Low MtCK expression in glycolytic muscles is another factor capable of influencing Cr-stimulated respiration. However, it was shown that the low expression of MtCK in *m. gastrocnemius* is related to the low volume that mitochondria occupy in this muscle fibers [46]. Fig. 1A shows that the maximal rate of Cr-stimulated respiration was identical for each muscle fiber-type with the maximal rate of ADP-stimulated respiration. This means that activated MtCK efficiently stimulates respiration in the absence of trapping system for ADP.

Fig. 3B shows that isolated heart mitochondria with low apparent Km for ADP (i.e. high apparent affinity of respiration for ADP) display high PK–PEP inhibition. In spite of saponin permeabilization, cardiomyocytes have high apparent K_m for ADP (i.e. low apparent affinity of respiration to ADP) and also low PK–PEP inhibition. In permeabilized cardiomyocytes and oxidative soleus muscle fibers the addition of PK–PEP inhibited Cr-stimulated respiration by only 2–5% of $V_{max(ATP + Cr)}$ (Fig. 3B). Very low inhibition of Cr-stimulated respiration in the presence of trapping system for ADP can be explained by restricted diffusion of adenine nucleotides at

Fig. 7. Confocal images of mitochondria and βII tubulin arrangement in fixed soleus muscle fibers. Optical slice of soleus fiber co-immunolabeled for VDAC (A) and α-actinin (B), and for VDAC (E) and βII tubulin (F). Images show that mitochondria and tubulin βII structures are arranged regularly between Z-lines. Higher magnification image highlights mitochondria (indicated by arrows) extending across the A-band. Optical sections presented here are obtained at least 0.5 μm beneath sarcolemma and specimens are oriented so that the long axis of the fiber is directed diagonally in upper-panel image longitudinally in the bottom-panel image. (Inset) Higher magnification image highlights mitochondria stalks (indicated by arrows) extending across the A-band. Scale bar 2 μM.

the level of MOM. These results confirm the hypothesis linking the apparent K_m for ADP and MOM permeability.

4.2. Study of energy fluxes in permeabilized skeletal muscle fibers using metabolic control analysis

Restricted diffusion of adenine nucleotides at the level of MOM in permeabilized cardiomyocytes increases mitochondrial compartmentation and control of respiration by creatine [1,2,4,7,12,19,30,47]. The role of MOM permeability in the distribution of mitochondrial energy flux in skeletal muscle fibers was studied using the method of metabolic control analysis [34–40]. The metabolic control analysis allows the estimation of the flux control coefficients that each metabolic pathway component exerts on the metabolic flux [34–36].

In oxidative soleus muscle fibers flux control coefficients of ATP synthase and ANT were higher under Cr- than ADP-stimulated respiration (Table 2). The increase of flux control coefficients under Cr-stimulated respiration was described previously for permeabilized cardiomyocytes and explained by the ADP-recycling in MtCK reaction [47]. In this case respiration was supported by small amounts of ADP continuously regenerated by MtCK within the intermembrane space which can be favored by two factors: MtCK-ANT functional coupling allowing direct ADP transfer to ATP synthase and adenine nucleotide micro-compartmentation due to their restricted diffusion through MOM. Due to high MOM permeability, initial flux of Cr-stimulated respiration of permeabilized GW muscle fibers measured after the addition of PK–PEP was lower than that of ADP-stimulated respiration making impossible comparison of flux control coefficients between both conditions for this muscle-type.

In the case of a linear metabolic pathway, the sum of FCCs does not exceed a unit [48,49]. In our experiments the sum of flux control coefficients of respiratory complexes (I, III and IV), ANT and ATP synthase estimated under conditions of ADP-stimulated respiration was higher than 1 in both permeabilized soleus and GW muscle fibers (Table 2). According to Lenaz et al., the sum of FCC exceeding unity can be explained by the spatial organization of respiratory complexes as supramolecular associations rather than randomly dispersed complexes in mitochondrial inner membrane [48,49]. According to the 3D molecular reconstruction of complexes I, III and IV, the ubiquinone and cytochrome c binding sites are facing each other favoring direct electron channeling [50,51]. Additional association of ATP synthase, ANT and phosphate carrier to the respiratory chain supercomplex was proposed by many authors [51–53] and used to explain the regulation of mitochondrial energy fluxes in cardiomyocytes [1,4]. One of the main properties of supramolecular assemblies is assumed to be the direct electron channeling between complexes resulting in the increase of oxidative phosphorylation efficiency, prevention of the excessive oxygen radical formation and stabilization of individual complexes by supramolecular assembly [51,53,54]. The supercomplex formation with direct electron flow between protein-bound CoQ instead of the lateral diffusion of CoQ is highly dependent on the properties and composition of membrane [55]. In spite of saponin permeabilization, there is no risk of supercomplexe formation due to the alteration of MIM fluidity. Saponin removes cholesterol from membranes due to its hydrophobic steroid core. The main constituent lipid of MIM is cardiolipin which cannot be removed by saponin. Otherwise inhibition of ADP-stimulated respiration up to V_0 by atractyloside was used to confirm the integrity of mitochondrial inner membrane.

4.3. Role of cytoskeletal proteins in regulation of respiration in skeletal muscle fibers

In spite of broadly similar structure and embedment of mitochondria into cytoskeleton in oxidative and glycolytic striated muscle fibers, the apparent affinity of mitochondrial respiration for ADP is different (Fig. 1B, Table 1). This difference, as we have shown above, depends on MOM permeability. Based on our previous results showing tubulin-dependent increase of the apparent K_m for ADP in isolated heart mitochondria [21–25], we hypothesized that MOM permeability in skeletal muscles could also be regulated by βII tubulin.

Bernier-Valentin was the first to show in 1982 that heterodimeric tubulin binds to VDAC decreasing MOM permeability to ADP in isolated heart mitochondria [56]. Further evidence for direct tubulin–mitochondria interaction came from co-immunoprecipitation experiments with different non-cancerous and cancerous cell lines evidencing complexation between tubulin and VDAC [57]. Finally, the influence of free tubulin on mitochondrial metabolism was showed in experiments with depolymerization of tubulin in cancerous hepatoma cells which increased mitochondrial membrane potential [58].
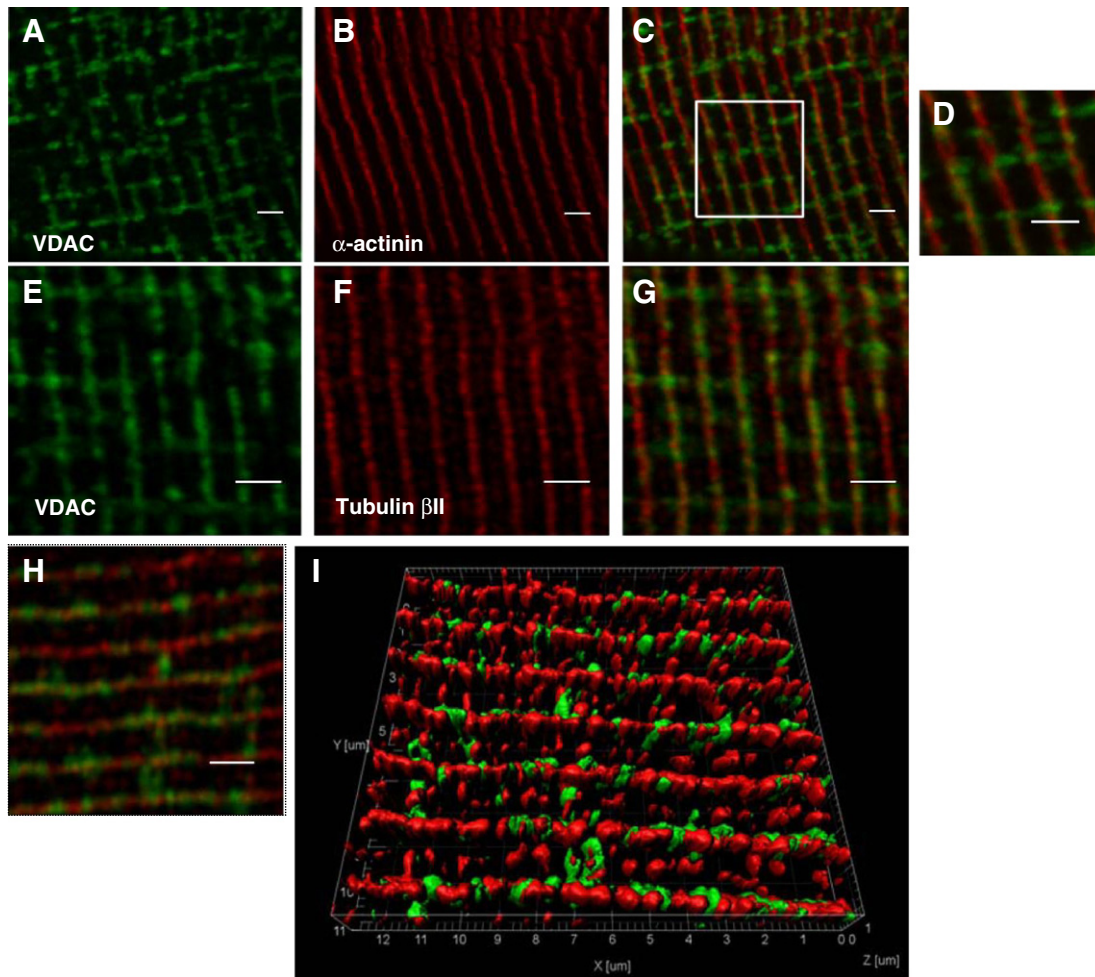
Fig. 8. Confocal images of mitochondrial and βII tubulin arrangement in fixed gastrocnemius white muscle fibers. Optical slices of GW fiber co-immunolabeled for VDAC (A) and α-actinin (B), and for VDAC (E) and βII tubulin (F) are obtained at least 0.5 μm beneath sarcolemma and specimens are all oriented so that the long axis of the fiber is directed longitudinally. Scale bar, 2 μm. Images show that mitochondria and βII tubulin are arranged close to Z-lines. Mitochondria highlighted in inset rarely extend across the A-band level. I) Three-dimensional reconstruction of confocal image represented in Fig. 7H. Fibers immunolabeled for VDAC and βII tubulin were scanned at 0.27 μm intervals along z-axis (maximum 10 planes, depending on the signal intensity) and 3D surface model was reconstructed by Imaris software (Bitplane). Scale bar, 2 μm. Image is oriented so that the long axis of the fiber is directed along y-axes and show continuous filaments of βII tubulin running along x-axis of image.

In our experiments, the expression of the total β tubulin accounting for non-polymerized and polymerized forms is in line with the results observed earlier, being higher in oxidative and lower in glycolytic muscles [59]. The expression of non-polymerized βII tubulin is high in heart and oxidative soleus muscle, low in the red portion of *m. gastrocnemius* and very low in the white portion of gastrocnemius and in EDL muscles (Fig. 5A, B). We hypothesized that free non-polymerized βII tubulin may participate in the regulation of MOM permeability in oxidative muscle fibers, while polymerized form of βII tubulin could be involved in mitochondrial organization. Evidence for the preferential expression of βII tubulin in tissues with oxidative phenotype has been reported already before. In addition to its abundance in heart and oxidative skeletal muscles, high expression of βII tubulin was found in brain and testis [60–62]. High expression of βII tubulin in synaptosomes was associated with high apparent K_m for ADP (about 110 μM in synaptosomes and about 10 μM in isolated brain mitochondria) [22]. Moreover the addition of heterodimeric tubulin increased the apparent K_m for ADP of isolated brain mitochondria as previously described in the case of isolated heart mitochondria [22].

Assessment of intracellular distribution of βII tubulin using immunofluorescent labeling revealed its presence in all studied muscles, including GW and EDL characterized by a very low level of the free βII tubulin expression (Figs. 6–8). In all studied muscles the distribution

of βII tubulin followed that of mitochondria. In soleus muscle fibers βII tubulin and VDAC immunofluorescent labelings were seen between Z-lines (Fig. 7), while in GW muscle fibers they were seen at the level of Z-lines (Fig. 8). The close proximity of βII tubulin to mitochondria in oxidative and glycolytic skeletal muscles regardless of their affinity to ADP (K_mADP) suggests that the intracellular distribution of this protein is not the main factor regulating the MOM permeability. The regulation of MOM permeability could be dependent on the expression of the dimeric fraction of βII tubulin.

How different muscle types achieve compartment specific targeting of mitochondria is to our knowledge largely uncovered. However it is well known that higher eukaryotes use predominantly microtubule (MT) tracks to distribute mitochondria. To realize location specific mitochondrial organization, a subset of MTs is exploited that distinguishes by their isoform composition, dynamic stability and post-translational modifications [63]. Therefore we hypothesized that βII tubulin subcellular arrangement could be associated with muscle type specific localization of mitochondria. To test this hypothesis, we compared localization of overall β-tubulin relative to α-actinin in soleus and in GW muscle fibers (Fig. 9A). We found that in soleus muscle fibers β-tubulin is concentrated in the area between Z-lines similarly to that of βII tubulin (Fig. 7F). Whereas in GW muscle fibers the two subpopulations of β-tubulins can be seen, one at the level of Z-lines, similarly to that of βII
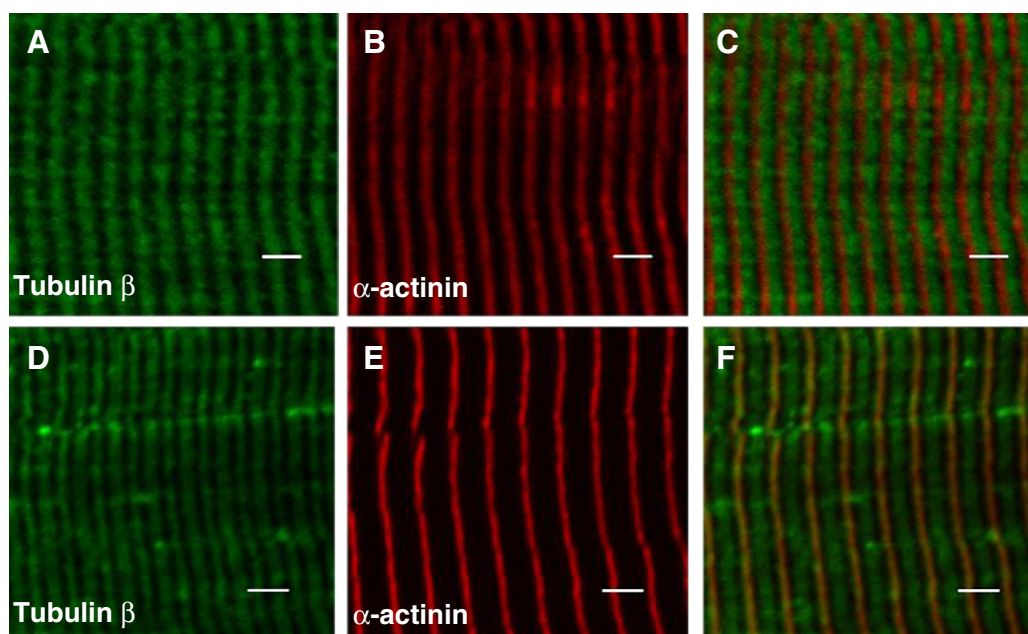
Fig. 9. Comparison of overall β-tubulin distribution relative to Z-lines in oxidative soleus and glycolytic GW skeletal muscle fibers. Optical slices of soleus (A–C) and GW (D–F) muscle fibers co-immunolabeled for VDAC (A, D) and α-actinin (B, E). In heart muscle fibers, transversely aligned β-tubulin stretches are located between Z-lines. In glycolytic GW muscle fibers, β-tubulin is present both between and along Z-lines. Scale bar 2 μm.

tubulin and second at the level of A-band (Fig. 9D). Thus, despite the presence of significant part of β-tubulin at the level of A-band in GW muscle fibers, mitochondria reside at the level of Z-lines (aligned along βII tubulin). These results support the idea that mitochondria position is defined by subset of microtubules that correlate in both muscle fiber types with organization of βII tubulin.

In live cells restriction of the adenine nucleotides diffusion through MOM is overcome by free diffusion of PCr which carries intracellular energy flux via the system of compartmentalized CK iso-enzymes [1,5,7,64]. Conversely, purified and reconstituted into planar phospholipid membrane VDAC in its closed state is impermeable for ATP, ADP and PCr [25]. Similar results were shown for isolated mitochondria from hematopoietic pro-B cell lines [65]. The selective permeability of VDAC depends on many factors, among which are the cell-specific pattern of VDAC iso-forms; VDAC interaction with different proteins (tubulin, HKII, MAP2, plectin, desmin …) regulated by distinct signaling cascades (growth factor or energy cascades); cell-specific pattern of intracellular proteins capable to interact with VDAC and their functional state (polymerization state or post-translational modifications, PTMs); biophysical properties of the channel itself, molecules going through the channel and MOM phospholipids [66]. All these aspects are component parts of the structural and functional organization of cellular energy metabolism oriented to support specific intracellular energy demanding processes such as the sarcomere contraction in highly differentiated cardiomyocytes or biosynthesis in actively growing and dividing cancer cells.

Differences in MOM permeability for ADP across muscle fiber types could stem from distinct expression patterns of VDAC isoforms. Striated muscles express three isoforms of VDAC [67]. According to Anflous-Pharayra et al., VDAC2 is mainly expressed in heart of wild-type murins and its deletion is embryologically lethal [68,69]. The decrease of the apparent affinity for ADP in permeabilized cardiac muscle fibers of VDAC1$^{-/-}$ mice and VDAC3$^{-/-}$ mice indicates the possible role of VDAC2 in the restriction of adenine nucleotide diffusion [68–70]. Interaction of microtubule-associated protein (MAP2) with VDAC2 [71] reinforces our belief that βII tubulin binds to VDAC2 regulating its permeability for phosphometabolites.

Glycolytic gastrocnemius muscle (mixture of red and white portions) of wild-type murins over-expresses VDAC1 [68] and VDAC3

[69] isoforms. VDAC1 and VDAC3 are permeable to ATP/ADP and this could be linked to the control by HKII [70,72]. VDAC1/3 null cells do not contain HKII bind to VDAC [73]. More studies are necessary to address the mechanism of regulation of the VDAC selective permeability.

Based on these results, we can link MOM permeability regulation with non-polymerized βII tubulin. Nevertheless it cannot be excluded that other β-tubulin or α-tubulin isoforms could also bind to VDAC and influence its conductance. At present the distribution of α-tubulins in muscle cells is totally uncovered and it is also unclear whether tubulin post-translational modifications could influence the interaction of tubulin with VDAC. The elucidation of these modification patterns in different skeletal muscles, could give an important contribution to unravel the complex interplay between microtubular network, metabolism, mitochondria dynamics and muscle contraction.

Conflict of interest

None of the co-authors of this article have any conflict of interest.

Acknowledgements

References

[1] V. Saks, A.V. Kuznetsov, M. Gonzalez-Granillo, K. Tepp, N. Timohhina, M. Karu-Varikmaa, T. Kaambre, P. Dos Santos, F. Boucher, R. Guzun, Intracellular energetic units regulate metabolism in cardiac cells, J. Mol. Cell. Cardiol. 52 (2012) 419–436.

[2] Molecular System Bioenergetics. Energy for Life, in: V. Saks (Ed.), Wiley-VCH, Weinheim Gmbh, Germany, 2007.

[3] V.A. Saks, T. Kaambre, P. Sikk, M. Eimre, E. Orlova, K. Paju, A. Piirsoo, F. Appaix, L. Kay, V. Regitz-Zagrosek, E. Fleck, E. Seppet, Intracellular energetic units in red muscle cells, Biochem. J. 356 (2001) 643–657.

[4] N. Timohhina, R. Guzun, K. Tepp, C. Monge, M. Varikmaa, H. Vija, P. Sikk, T. Kaambre, D. Sackett, V. Saks, Direct measurement of energy fluxes from mitochondria into

cytoplasm in permeabilized cardiac cells in situ: some evidence for mitochondrial interactosome, J. Bioenerg. Biomembr. 41 (2009) 259–275.

[5] V. Saks, R. Guzun, N. Timohhina, C. Monge, M. Varikmaa, H. Vija, P. Sikk, T. Kaambre, D. Sackett, V. Saks, Structure–function relationships in feedback regulation of energy fluxes in vivo in health and disease: mitochondrial interactosome, Biochim. Biophys. Acta 1797 (2010) 678–697.

[6] P. Pedersen, Transport ATPases into the year 2008: a brief overview related to types, structures, functions and roles in health and disease, J. Bioenerg. Biomembr. 39 (2007) 349–355.

[7] T. Wallimann, M. Wyss, D. Brdiczka, K. Nicolay, H.M. Eppenberger, Intracellular compartmentation, structure and function of creatine kinase isoenzymes in tissues with high and fluctuating energy demands: the "phosphocreatine circuit" for cellular energy homeostasis, Biochem. J. 281 (1992) 21–40.

[8] L. Kay, K. Nicolay, B. Wieringa, V. Saks, T. Wallimann, Direct evidence for the control of mitochondrial respiration by mitochondrial creatine kinase in oxidative muscle cells in situ, J. Biol. Chem. 275 (2000) 6937–6944.

[9] V. Saks, P. Dzeja, U. Schlattner, M. Vendelin, A. Terzic, T. Wallimann, Cardiac system bioenergetics: metabolic basis of the Frank–Starling law, J. Physiol. 571 (2006) 253–273.

[10] S. Schiaffino, C. Reggiani, Molecular diversity of myofibrillar proteins: gene regulation and functional significance, Physiol. Rev. 76 (1996) 371–423.

[11] M.D. Delp, C. Duan, Composition and size of type I, IIA, IID/X, and IIB fibers and citrate synthase activity of rat muscle, J. Appl. Physiol. 80 (1996) 261–270.

[12] A.V. Kuznetsov, T. Tiivel, P. Sikk, T. Kaambre, L. Kay, Z. Daneshrad, A. Rossi, L. Kadaja, N. Peet, E. Seppet, V.A. Saks, Striking differences between the kinetics of regulation of respiration by ADP in slow-twitch and fast-twitch muscles in vivo, Eur. J. Biochem. 241 (1996) 909–915.

[13] E. Barth, G. Stämmler, B. Speiser, J. Schaper, Ultrastructural quantitation of mitochondria and myofilaments in cardiac muscle from 10 different animal species including man, J. Mol. Cell. Cardiol. 24 (1992) 669–681.

[14] T. Ogata, Y. Yamasaki, Ultra-high-resolution scanning electron microscopy of mitochondria and sarcoplasmic reticulum arrangement in human red, white, and intermediate muscle fibers, Anat. Rec. 248 (1997) 214–223.

[15] M. Picard, R.T. Hepple, Y. Burelle, Mitochondrial functional specialization in glycolytic and oxidative muscle fibers: tailoring the organelle for optimal function, Am. J. Physiol. Cell Physiol. 302 (2012) C629–C641.

[16] R.B. Armstrong, R.O. Phelps, Muscle fiber type composition of the rat hindlimb, Am. J. Anat. 171 (1984) 259–272.

[17] B. Glancy, R.S. Balaban, Protein composition and function of red and white skeletal muscle mitochondria, Am. J. Physiol. Cell Physiol. 300 (2011) C1280–C1290.

[18] L. Kay, Z. Li, M. Mericskay, J. Olivares, L. Tranqui, E. Fontaine, T. Tiivel, P. Sikk, T. Kaambre, J.L. Samuel, L. Rappaport, Y. Usson, X. Leverve, D. Paulin, V.A. Saks, Study of regulation of mitochondrial respiration in vivo. An analysis of influence of ADP diffusion and possible role of cytoskeleton, Biochim. Biophys. Acta 1322 (1997) 41–59.

[19] V.A. Saks, A.V. Kuznetsov, Z.A. Khuchua, E.V. Vasilyeva, J.O. Belikova, T. Kesvatera, T. Tiivel, Control of cellular respiration in vivo by mitochondrial outer membrane and by creatine kinase. A new speculative hypothesis: possible involvement of mitochondrial–cytoskeleton interactions, J. Mol. Cell. Cardiol. 27 (1995) 625–645.

[20] V.A. Saks, V.I. Veksler, A.V. Kuznetsov, L. Kay, P. Sikk, T. Tiivel, L. Tranqui, J. Olivares, K. Winkler, F. Wiedemann, W.S. Kunz, Permeabilized cell and skinned fiber techniques in studies of mitochondrial function in vivo, Mol. Cell. Biochem. 184 (1998) 81–100.

[21] T.K. Rostovtseva, K.L. Sheldon, E. Hassanzadeh, C. Monge, V. Saks, S.M. Bezrukov, D.L. Sackett, Tubulin binding blocks mitochondrial voltage-dependent anion channel and regulates respiration, Proc. Natl. Acad. Sci. U. S. A. 105 (2008) 18746–18751.

[22] C. Monge, N. Beraud, A.V. Kuznetsov, T. Rostovtseva, D. Sackett, U. Schlattner, M. Vendelin, V.A. Saks, Regulation of respiration in brain mitochondria and synaptosomes: restrictions of ADP diffusion in situ, roles of tubulin, and mitochondrial creatine kinase, Mol. Cell. Biochem. 318 (2008) 147–165.

[23] T.K. Rostovtseva, S.M. Bezrukov, VDAC regulation: role of cytosolic proteins and mitochondrial lipids, J. Bioenerg. Biomembr. 40 (2008) 163–170.

[24] T.K. Rostovtseva, Control of mitochondrial outer membrane permeability: VDAC regulation by dimeric tubulin and cytosolic proteins, in: O.L. Svensson (Ed.), Mitochondria: Structure, Functions and Dysfunctions, Nova Biomedical Books, New York, 2010, pp. 607–634.

[25] T.K. Rostovtseva, S.M. Bezrukov, VDAC inhibition by tubulin and its physiological implications, Biochim. Biophys. Acta 1818 (2012) 1526–1535.

[26] M. Gonzalez-Granillo, A. Grichine, R. Guzun, Y. Usson, K. Tepp, V. Chekulayev, I. Shevchuk, M. Karu-Varikmaa, A.V. Kuznetsov, M. Grimm, V. Saks, T. Kaambre, Studies of the role of tubulin beta II isotype in regulation of mitochondrial respiration in intracellular energetic units in cardiac cells, J. Mol. Cell. Cardiol. 52 (2012) 437–447.

[27] R. Guzun, M. Karu-Varikmaa, M. Gonzalez-Granillo, A.V. Kuznetsov, L. Michel, C. Cottet-Rousselle, M. Saaremae, T. Kaambre, M. Metsis, M. Grimm, C. Auffray, V. Saks, Mitochondria–cytoskeleton interaction: distribution of beta-tubulins in cardiomyocytes and HL-1 cells, Biochim. Biophys. Acta 1807 (2011) 458–469.

[28] A.V. Kuznetsov, V. Veksler, F.N. Gellerich, V. Saks, R. Margreiter, W.S. Kunz, Analysis of mitochondrial function in situ in permeabilized muscle fibers, tissues and cells, Nat. Protoc. 3 (2008) 965–976.

[29] A.V. Kuznetsov, R. Guzun, F. Boucher, R. Bagur, T. Kaambre, V.A. Saks, Mysterious Ca^{2+}-independent muscular contraction: déjà vu, Biochem. J. 445 (2012) 333–336.

[30] R. Guzun, N. Timohhina, K. Tepp, C. Monge, T. Kaambre, P. Sikk, A.V. Kuznetsov, C. Pison, V. Saks, Regulation of respiration controlled by mitochondrial creatine kinase in permeabilized cardiac cells in situ. Importance of system level properties, Biochim. Biophys. Acta 1787 (2009) 1089–1105.

[31] E. Gnaiger, Oxygen Solubility in Experimental Media, OROBOROS Bioenergetics Newsletter MiPNet 6.3, Innsbruck, Austria, 2001.

[32] F. Appaix, M. Minatchy, C. Riva-Lavieille, J. Olivares, B. Antonsson, V.A. Saks, Rapid spectrophotometric method for quantitation of cytochrome c release from isolated mitochondria or permeabilized cells revisited, Biochim. Biophys. Acta 1457 (2000) 175–181.

[33] C.G.R. Perry, D.A. Kane, C.T. Lin, R. Kozy, B.L. Cathey, D.S. Lark, C.L. Kane, P.M. Brophy, T.P. Gavin, E.J. Anderson, P.D. Neufer, Inhibiting myosin-ATPase reveals a dynamic range of mitochondrial respiratory control in skeletal muscle, Biochem. J. 437 (2011) 215–222.

[34] A.K. Groen, R.J. Wanders, H.V. Westerhoff, R. van der Meer, J.M. Tager, Quantification of the contribution of various steps to the control of mitochondrial respiration, J. Biol. Chem. 257 (1982) 2754–2757.

[35] D.A. Fell, Metabolic control analysis: a survey of its theoretical and experimental development, Biochem. J. 286 (1992) 313–330.

[36] R. Moreno-Sanchez, E. Saavedra, S. Rodriguez-Enriquez, V. Olin-Sandoval, Metabolic control analysis: a tool for designing strategies to manipulate metabolic pathways, J. Biomed. Biotechnol. (2008) 597913.

[37] E. Wisniewski, F.N. Gellerich, W.S. Kunz, Distribution of flux control among the enzymes of mitochondrial oxidative phosphorylation in calcium-activated saponin-skinned rat musculus soleus fibers, Eur. J. Biochem. 230 (1995) 549–554.

[38] A.V. Kuznetsov, K. Winkler, E. Kirches, H. Lins, H. Feistner, W.S. Kunz, Application of inhibitor titrations for the detection of oxidative phosphorylation defects in saponin-skinned muscle fibers of patients with mitochondrial diseases, Biochim. Biophys. Acta 1360 (1997) 142–150.

[39] W.S. Kunz, A. Kudin, S. Vielhaber, C.E. Elger, G. Attardi, G. Villani, Flux control of cytochrome c oxidase in human skeletal muscle, J. Biol. Chem. 275 (2000) 27741–27745.

[40] A.J. Fritzen, N. Grunnet, B. Quistorff, Flux control analysis of mitochondrial oxidative phosphorylation in rat skeletal muscle: pyruvate and palmitoyl-carnitine as substrates give different control patterns, Eur. J. Appl. Physiol. 101 (2007) 679–689.

[41] T. Tashiro, J. Komiya, Stable and dynamic forms of cytoskeletal proteins in slow axonal transport, J. Neurosci. 9 (1989) 760–768.

[42] A. Banerjee, M.C. Roach, K.A. Wall, M.A. Lopata, D.W. Cleveland, R.F. Ludueña, A monoclonal antibody against the type II isotype of beta-tubulin. Preparation of isotypically altered tubulin, J. Biol. Chem. 263 (1988) 3029–3034.

[43] F. Appaix, A.V. Kuznetsov, Y. Usson, L. Kay, T. Andrienko, J. Olivares, T. Kaambre, P. Sikk, R. Margreiter, V. Saks, Possible role of cytoskeleton in intracellular arrangement and regulation of mitochondria, Exp. Physiol. 88 (2003) 175–190.

[44] F.N. Gellerich, M. Schlame, V.A. Saks, Creatine kinase of heart mitochondria: no changes in its kinetic properties after inhibition of the adenine nucleotide translocator, Biomed. Biochim. Acta 42 (1983) 1335–1337.

[45] A. Lin, G. Krockmalnic, S. Penman, Imaging cytoskeleton–mitochondrial membrane attachments by embedment-free electron microscopy of saponin-extracted cells, Proc. Natl. Acad. Sci. U. S. A. 87 (1990) 8565–8569.

[46] W.N. Qin, Z. Khuchua, J. Boero, R.M. Payne, A.W. Strauss, Oxidative myocytes of heart and skeletal muscle express abundant sarcomeric mitochondrial creatine kinase, Histochem. J. 31 (1999) 357–365.

[47] K. Tepp, N. Timohhina, V. Chekulayev, I. Shevchuk, T. Kaambre, V. Saks, Metabolic control analysis of integrated energy metabolism in permeabilized cardiomyocytes — experimental study, Acta Biochim. Pol. 57 (2010) 421–430.

[48] G. Lenaz, M.L. Genova, Structure and organization of mitochondrial respiratory complexes: a new understanding of an old subject, Antioxid. Redox Signal. 12 (2010) 961–1008.

[49] G. Lenaz, A. Baracca, G. Barbero, C. Bergamini, M.E. Dalmonte, M. Del Sole, M. Faccioli, A. Falasca, R. Fato, M.L. Genova, G. Sgarbi, G. Solaini, Mitochondrial respiratory chain super-complex I–III in physiology and pathology, Biochim. Biophys. Acta 1797 (2010) 633–640.

[50] J. Vonck, E. Schäfer, Supramolecular organization of protein complexes in the mitochondrial inner membrane, Biochim. Biophys. Acta 1793 (2009) 117–124.

[51] E. Schäfer, N.A. Dencher, J. Vonck, D.A. Parcej, Three-dimensional structure of the respiratory chain supercomplex $I_1III_2IV_1$ from bovine heart mitochondria, Biochemistry 46 (2007) 12579–12585.

[52] H. Schägger, K. Pfeiffer, The ratio of oxidative phosphorylation complexes I–V in bovine heart mitochondria and the composition of respiratory chain supercomplexes, J. Biol. Chem. 276 (2001) 37861–37867.

[53] H. Schägger, R. de Coo, M.F. Bauer, S. Hofmann, C. Godinot, U. Brandt, Significance of respirasomes for the assembly/stability of human respiratory chain complex I, J. Biol. Chem. 279 (2004) 36349–36353.

[54] M.L. Genova, A. Baracca, A. Biondi, G. Casalena, M. Faccioli, A.I. Falasca, G. Formiggini, G. Sgarbi, G. Solaini, G. Lenaz, Is supercomplex organization of the respiratory chain required for optimal electron transfer activity? Biochim. Biophys. Acta 1777 (2008) 740–746.

[55] C.R. Hackenbrock, B. Chazotte, S.S. Gupte, The random collision model and a critical assessment of diffusion and collision in mitochondrial electron transport, J. Bioenerg. Biomembr. 18 (1986) 331–368.

[56] F. Bernier-Valentin, B. Rousset, Interaction of tubulin with rat liver mitochondria, J. Biol. Chem. 257 (1982) 7092–7099.

[57] M. Carre, N. Andre, G. Carles, H. Borghi, L. Brichese, C. Briand, D. Braguer, Tubulin is an inherent component of mitochondrial membranes that interacts with the voltage-dependent anion channel, J. Biol. Chem. 277 (2002) 33664–33669.

[58] E.N. Maldonado, J. Patnaik, M.R. Mullins, J.J. Lemasters, Free tubulin modulates mitochondrial membrane potential in cancer cells, Cancer Res. 70 (2010) 10192–10201.

[59] K. Guerrero, C. Monge, A. Brückner, Ü. Puurand, L. Kadaja, T. Käämbre, E. Seppet, V. Saks, Study of possible interactions of tubulin, microtubular network, and STOP protein with mitochondria in muscle cells, Mol. Cell. Biochem. 37 (2009) 239–249.

[60] L.J. Leandro-Garcia, S. Leskelä, I. Landa, C. Montero-Conde, E. Lopez-Jimenez, R. Leton, A. Cadcon, M. Robledo, C. Rodriguez-Antona, Tumoral and tissue-specific expression of the major human b-tubulin isotypes, Cytoskeleton 67 (2010) 214–223.

[61] Y.M. Nakamura, E. Oda, A. Yamamoto, Y. Kanemura, M. Hara, A. Suzuki, M. Yamasaki, H. Okano, Expression of tubulin beta II in neural stem/progenitor cells and radial fibers during human fetal brain development, Lab. Invest. 83 (2003) 479–489.

[62] T. Narishige, K.L. Blade, Y. Ishibashi, T. Nagai, M. Hamawaki, D.R. Menick, D. Kuppuswamy, G. Cooper IV, Cardiac hypertrophic and developmental regulation of the β-tubulin multigene family, J. Biol. Chem. 274 (1999) 9692–9697.

[63] A.F. MacAskill, J.T. Kittler, Control of mitochondrial transport and localization in neurons, Trends Cell Biol. 20 (2010) 102–112.

[64] U. Schlattner, M. Tokarska-Schlattner, T. Wallimann, Mitochondrial creatine kinase in human health and disease, Biochim. Biophys. Acta 1762 (2006) 164–180.

[65] M.G. Vander Heiden, N.S. Chandel, X.X. Li, P.T. Schumacker, M. Colombini, C.B. Thompson, Outer mitochondrial membrane permeability can regulate coupled respiration and cell survival, Proc. Natl. Acad. Sci. U. S. A. 97 (2000) 4666–4671.

[66] T.K. Rostovtseva, P.A. Gurnev, M.Y. Chen, S.M. Bezrukov, Membrane lipid composition regulates tubulin interaction with mitochondrial voltage-dependent anion channel, J. Biol. Chem. 287 (2012) 29589–29598.

[67] V. De Pinto, F. Guarino, A. Guarnera, A. Messina, S. Reina, F.M. Tomasello, V. Palermo, C. Mazzoni, Characterization of human VDAC isoforms: a peculiar function for VDAC3? Biochim. Biophys. Acta 1797 (2010) 1268–1275.

[68] K. Anflous, D.D. Armstrong, W.J. Craigen, Altered mitochondrial sensitivity for ADP and maintenance of creatine-stimulated respiration in oxidative striated muscles from VDAC-1 deficient mice, J. Biol. Chem. 276 (2001) 1954–1960.

[69] K. Anflous-Pharayra, N. Lee, D.L. Armstrong, W.J. Craigen, VDAC2 has different mitochondrial functions in two types of striated muscles, Biochim. Biophys. Acta 1807 (2011) 150–156.

[70] K. Anflous-Pharayra, Z.J. Cai, W.J. Craigen, VDAC1 serves as a mitochondrial binding site for hexokinase in oxidative muscles, Biochim. Biophys. Acta 1767 (2007) 136–142.

[71] M. Linden, B.D. Nelson, D. Loncar, J.F. Leterrier, Studies on the interaction between mitochondria and the cytoskeleton, J. Bioenerg. Biomembr. 21 (1989) 507–518.

[72] E.N. Maldonado, J.J. Lemasters, Warburg revisited: regulation of mitochondrial metabolism by voltage-dependent anion channels in cancer cells, J. Pharmacol. Exp. Ther. 342 (2012) 637–641.

[73] F. Chiara, D. Castellaro, O. Marin, V. Petronilli, W.S. Brusilow, M. Juhaszova, S.J. Solott, M. Forte, P. Bernardi, A. Rasola, Hexokinase II detachment from mitochondria triggers apoptosis through the permeability transition pore independent of voltage-dependent anion channels, PLoS One 3 (2008) e1852.